

Evaluating an Image Based Multi-angle BRDF Measurement Setup

ADITYA SOLE^{1,*}, IVAR FARUP¹, PETER NUSSBAUM¹, AND SHOJI TOMINAGA^{1,2}

¹The Norwegian Colour and Visual Computing Laboratory, Department of Computer Science, Faculty of Information technology and Electrical engineering, Norwegian University of Science and Technology

²Graduate School of Advanced Integration Science, Chiba University, Chiba, Japan

* Corresponding author: aditya.sole@ntnu.no

Compiled January 31, 2018

We evaluate an image based multi-angle BRDF measurement setup by comparing it against measurements from two commercially available table top gonio-spectrophotometers. The image based setup uses an RGB camera to perform bidirectional measurements of the sample material. We use a conversion matrix to calculate luminance from the captured data. The matrix is calculated using camera spectral sensitivities that are measured with a monochromator. Radiance factor of the sample material is measured using commercially available tabletop gonio-spectrophotometer and compared against measurements made using the image based setup in the colorimetric domain. Our measurement setup is validated by comparing the measurements performed using a gonio-spectrophotometer. Uncertainty and error propagation is calculated and taken into account for validation. The sample material measured is wax based ink printed on packaging paper substrate commonly used in print and packaging industry. Results obtained show that the image based setup can perform bidirectional reflectance measurements with a known uncertainty. The gonio-spectrophotometer measurements lie within the uncertainty of the measurements performed by the image based measurement setup. The setup can be used to perform bi-directional reflectance measurements on samples with properties similar to the samples used in this article. © 2018 Optical Society of America

OCIS codes: 330.0330, 330.1710

<http://dx.doi.org/10.1364/ao.XX.XXXXXX>

1. INTRODUCTION

The quality of an object is often judged by its total appearance. To describe the physical correlates to the total appearance of an object (whether it is food, textile, skin, chemicals, coatings, metals, paper, plastics) optical properties are measured. The overall appearance of an object/material is resulting from a combination of its chromatic attributes (colour described in terms of lightness, hue, and saturation) and its geometric attributes (like gloss, translucency and texture) [1].

In recent years, various technologies (like effect inks [2] or conventional inks printed on metallic foils [3]) have been introduced particularly in the packaging industry to create appearance effects. These inks, however, cannot be described well enough by conventional measurements using a single measurement geometry.

For such materials the reflection of light is not satisfactorily modelled as, e.g., a lambertian surface where the intensity of the light is proportional to the cosine of the reflection angle. They produce a desirable appearance by changing their perceived

colour or lightness properties with a change in illumination and viewing direction [4]. In order to characterise and reproduce such a material, reflectance measurements are performed at different illumination and viewing directions [4]. Back in 2007, Takagi et al. [5] stated that to characterise the reflection properties of special effect coatings, measurements taken at as many as 1485 different measurement geometries are required. It is practically very difficult to perform these measurements and use such a huge data for processing. Krichner and Werner [6] demonstrated that a reduction in number of measurement geometries is essential and is possible with physical interpretation of the amount of light reflected at different measurement geometries. A recent study made by Ferrero et. al [7], to characterise the color shift of special effect coatings shows that a maximum of 10 geometries could be sufficient.

For traditional colour pigments that are printed on diffuse paper substrates, traditional measurement geometries recommended by CIE [8] are sufficient to characterise the materials in a way that correlates well with how the colour of the material

is perceived. In graphic arts and print industry, measuring instruments with $45^\circ:0^\circ$ geometry are widely used for reflectance measurement of materials. Sphere based geometries are mainly used in the paint, textile and plastic industries. For non-diffuse materials like metallic inks the incident light is specularly reflected. ASTM standards [9, 10] recommend the illumination and viewing directions for measurement of a few different types of the non-diffuse materials. Integrating sphere based measurement instruments are often used to measure non-diffuse samples. However, using an integrating sphere based instrument is not sufficient as it captures an average colorimetry of the sample and not the detailed angular variation of the reflected light. According to [4, 11], using the traditional single geometry measurement instruments are also non-sufficient to measure and characterise such non-diffuse materials. Measurements made at more than one illumination and viewing directions are therefore required to characterise such materials.

Instruments measuring at a few selected multiple fixed directions are termed as multi-angle spectrophotometer [12] whereas instruments that are used for measurements over a broad range of angles are called gonio-spectrophotometers. In this article, we adopt the terminology 'gonio-spectrophotometer' to describe any instrument that performs measurements at more than one illumination and viewing direction.

A number of gonio-spectrophotometers are commercially available and widely used to perform measurements at different illumination and viewing directions [13]. These instruments measure the sample material spectrally at different illumination and viewing directions. The measurement quantity obtained is the ratio of the reflected and incident power (Φ_r / Φ_i). Using this measurement quantity the bidirectional reflectance distribution function (BRDF), f_r of the material can be computed. Spectral radiant power and the corresponding radiometric terms required to express a BRDF are well defined and can be referred in [14], and the BRDF is defined by Nicodemus et. al [15] as:

$$f_r(\theta_i, \phi_i, \theta_r, \phi_r, \lambda) = \frac{dL_r(\theta_i, \phi_i, \theta_r, \phi_r, \lambda)}{dE_i(\theta_i, \phi_i, \lambda)} \quad (1)$$

where, $L_r(\theta_i, \phi_i, \theta_r, \phi_r, \lambda)$ is the reflected radiance in the direction (θ_r, ϕ_r) , and $E_i(\theta_i, \phi_i, \lambda)$ is the irradiance from the direction (θ_i, ϕ_i) . The illumination and viewing direction are described relative to the surface normal, so-called 'anormal angle', in agreement with the ASTM E2175-01 [12] standard and the CIE 175 [16] technical report.

A gonio-spectrophotometer can measure at a broad number of illumination and viewing angles, but, are slow. One of the main reasons for this is that they require the sample material to be measured lying flat while the detector and the light source or the sample rotates to perform bidirectional measurements. The geometrical calibration for the detector and light source or sample surface rotation, and the spectral calibration of the incident light source contributes heavily to the measurement time of the instrument.

In order to overcome these drawbacks, image based measurement setups have been proposed and presented in the past [17] to perform bidirectional measurements of flexible thin materials like print and packaging paper or plastic. Our setup used in this study can perform measurements fast (in a single shot) and in-line with production of such print and packaging materials which can be an advantage against gonio-spectrophotometers. Guarniera et. al [18] provided an overview of measuring instruments that are used for bidirectional measurements.

Sole et. al [19, 20] uses such a setup to measure thin flexible materials (printed packaging paper). The measured data is then used to train different reflection models (for example Cook-Torrance). In [21], Sole et al. trained two reflection models with measurement data captured using the image based measurement setup described in [19, 22]. One of the sample material was also measured using a Minolta CS1000 tele-spectro-radiometer (TSR) at 4 different viewing directions for a given illumination direction. Using the trained reflection models, CIEXYZ Y value for the sample material was estimated at these 4 viewing directions for the given illumination direction. These estimated CIEXYZ Y values were then compared with the TSR measured CIEXYZ Y values. It was observed that the measurements performed using the TSR were not precise in terms of geometrical conditions (illumination and viewing angles). Also the measurements used for training the reflection models and to test, were generated from the same setup.

Although several image-based setups have been proposed in the past, it is not well established how accurately they perform in comparison with gonio-spectrophotometers. In this article, we use an the existing image based measurement setup from [19] and compare the results with two commercially available gonio-spectrophotometers by transforming the results into a common domain. This is performed for printed packaging paper material samples. We use the terminology 'our measurement setup' when referring to the image based setup from [19]. Secondly, we investigate the accuracy of the image-based setup by means of a propagation-of-error analysis.

2. METHOD

In this article we evaluate image based measurement setup used in [19] using commercially available gonio-spectrophotometer for bidirectional measurements of thin flexible materials. 4 material samples (from print and packaging industry) named LightCyan (LC) and LightMagenta (LM), Cyan (C) and Magenta (M) are measured using our measurement setup and two commercially available gonio-spectrophotometers PerkinElmer's *LAMBDA1050* (referred as '*LAMBDA1050*') and Murakami's GCMS-3B Gonio-Spectrophotometric Color Measurement Systems (referred as '*GCMS*'). To evaluate our measurement setup, we use sample materials printed on matt coated paper with wax based inks using an OCE ColorWave600 plotter. Spectralon tile was measured with *LAMBDA1050* and captured with our measurement setup along with the samples. As the samples were solid colour patches printed on packaging paper material, they are homogeneous and flexible.

A. Measurements

Out of the four samples, two samples, LightCyan (LC) and LightMagenta (LM), were measured using *LAMBDA1050* while samples Cyan (C) and Magenta (M) were measured using *GCMS*. The spectralon tile (ST) was measured using *LAMBDA1050* along with LC and LM samples. Appendix describes both the gonio-spectrophotometers of their design and measurement output.

For *LAMBDA1050*, the measurement output is the ratio of reflected radiant flux to incident radiant flux (Φ_r / Φ_i). Radiance factor (β_r) is calculated from the measured output using Equation (2) [23].

$$\beta_r(\lambda) = \frac{\Phi_r(\lambda)}{\Phi_i(\lambda)} \cdot \frac{\pi}{\omega_r \cos \theta_r} \quad (2)$$

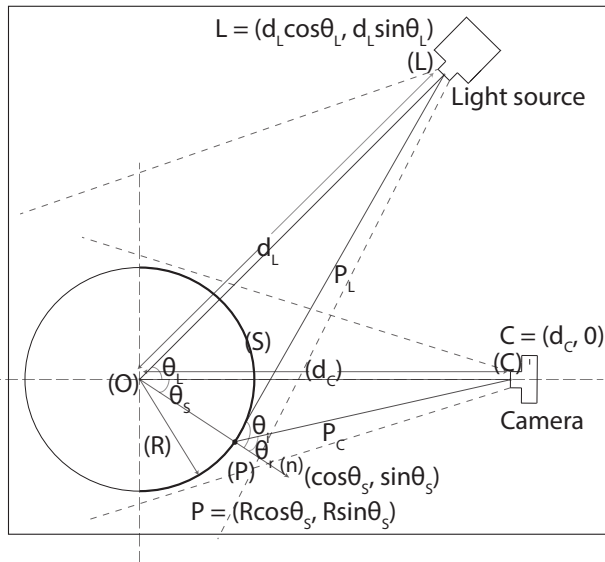


Fig. 1. Measurement setup in a vector plane [Image reproduced with permission [19]]

where, ω_r is the detector solid angle, and θ_r is the anormal viewing angle.

The measurement output of GCMS is the radiance factor (β_r). The BRDF can further be calculated using $f_r = \frac{\beta_r}{\pi}$ relation.

Our measurement setup uses a point light source and a commercially available digital camera as a detector. The light source and the detector is at a fixed position from the sample (for example light source at 45° and detector at 0°) and the measurement sample is curved onto a cylinder of known radius. Figure (1) shows the setup in a vector plane. As described in [19] and referring to Figure (1), point C is the detector position (digital camera position) approximately at the center of the curved sample at a distance d_C . L is a point light source illuminating the sample at a fixed angle $\theta^\circ < \theta_L < 90^\circ$ at a known distance d_L from the center of the curved sample. Assuming that the curved sample is homogeneous, light incident and reflected at any given point on the sample provides information with respect to the light source position (L), camera (C) and the surface normal vector (\mathbf{n}) at point P. θ_i and θ_r are incident and reflection angles with respect to the normal \mathbf{n} at a given point (P). Considering the setup in a vector plane, θ_i and θ_r are calculated as given in Equation (3)

$$\cos \theta_i = \frac{\mathbf{P}_L \cdot \mathbf{n}}{|\mathbf{P}_L|}, \quad \cos \theta_r = \frac{\mathbf{P}_C \cdot \mathbf{n}}{|\mathbf{P}_C|} \quad (3)$$

As the measurements are performed using a digital camera, each pixel in the captured image corresponds to point (P) on the curved sample surface. As each point (P) (on the sample) makes a corresponding incident (θ_i) and reflection (θ_r) angle with respect to the normal (\mathbf{n}) at point (P), the information recorded by each pixel corresponds to a bidirectional measurement at point (P).

As discussed in [22], the captured image records the light information in digital values for each camera sensor. The measured camera spectral sensitivities ($r(\lambda)$, $g(\lambda)$, $b(\lambda)$) along with CIE 2° colour matching functions (\bar{x} , \bar{y} , \bar{z}) are used to calculate a 3×3 matrix, \hat{M} . Using \hat{M} , the captured RGB data can be converted into a colorimetric space (CIEXYZ).

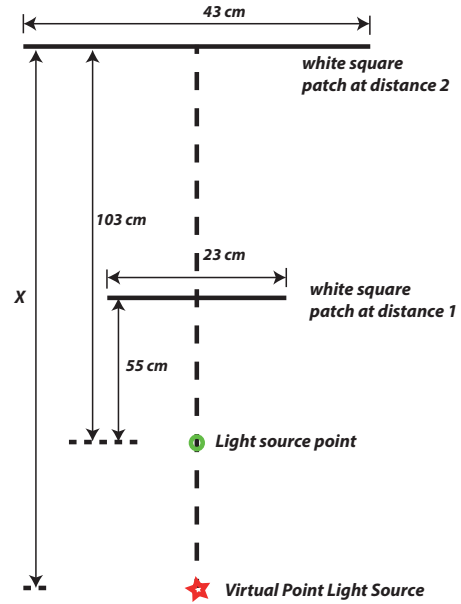


Fig. 2. Virtual point light source calculation

Samples LC, LM and ST, were measured at three anormal incident ($\theta_i = 25^\circ, 35^\circ, 45^\circ$) and 26 anormal reflection angles (ranging between $\theta_r = [+75^\circ, -75^\circ]$ at 5° intervals) using LAMBDA1050. A ratio of the reflected radiant flux to incident flux (Φ_r/Φ_i) in the range of 380 nm to 730 nm at 10 nm intervals was recorded. We calculate the radiance factor using equation (2). The distance between the sample and the detector was 91 mm, while the detector aperture area was 12.7 mm x 15.5 mm thus giving a solid angle (ω_r) of 0.0237 sr [24].

Similarly, samples C and, M were measured using GCMS. Spectral radiance factor is recorded in the range of 390 nm - 730 nm at 10 nm interval at anormal incident (θ_i) and reflection (θ_r) angles in the range of $[+80^\circ, -80^\circ]$ at 5° intervals.

In our measurement setup, sample is illuminated using a tungsten point light source, and was captured using a 16 bit Nikon D200 DSLR camera. As a point light source we use a film projector (consisting of a halogen tungsten lamp). As the projector uses a focusing lens, using inverse square law we calculate the origin of the point light source by illuminating a white patch at 2 distance intervals and measure the illuminated area of the white patch and distance between the projector and the illuminated surface. Figure 2 shows a schematic diagram of the setup and measurements. Referring to Figure 2, distance x is calculated as 103.2 cm. The homogeneity of the light source was checked by measuring the incident light at different parts of the given sample area. The incident beam was homogeneous with a variation of approximately 7.2% across an area of size 10cm x 5cm at the sample surface.

As a white reference, ST is used in the setup. Illumination and viewing angles are calculated for each pixel point (p) that corresponds to the given point (P) on the curved sample. As discussed in [19], for a given illumination direction (θ_i), the number of viewing directions that we can measure will depend on the sample curvature, resolution of the digital camera used as detector and the distance between the curved sample and the detector. Also, as we measure the curved sample at different illumination directions (θ_i), the area illuminated on the curved sample

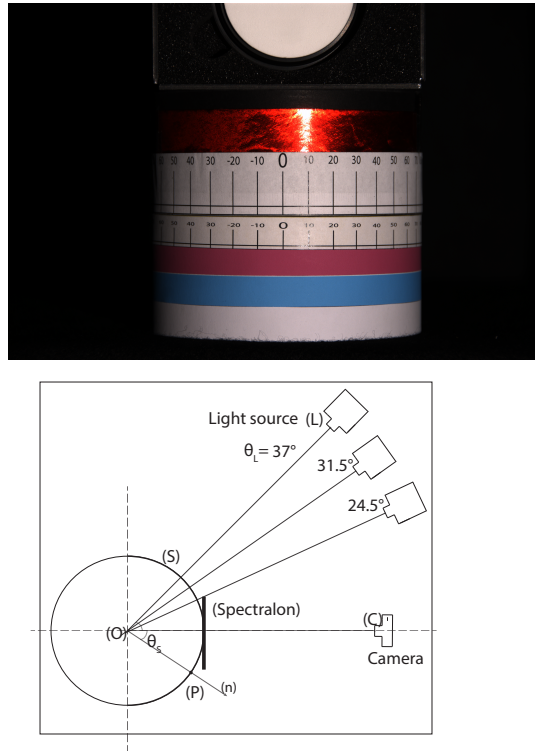


Fig. 3. LC and LM sample measurement at 3 different illumination directions (θ_L) and image captured at $\theta_L = 24.5^\circ$

changes with change in θ_L . It is therefore important to consider the viewing angles in the area which is uniformly illuminated with all the illumination directions for further processing and comparison.

LC and LM samples were measured at three different illumination directions ($\theta_L = 24.5^\circ, 31.5^\circ, 37^\circ$) using our measurement setup (refer Figure 3). Figure 3 shows the image captured at $\theta_L = 24.5^\circ$. C and M samples were measured at seven different illumination directions ($\theta_L = 15^\circ, 18^\circ, 20^\circ, 25^\circ, 28^\circ, 30^\circ$, and 35°) (refer Figure 4). Figure 4 shows the image captured at $\theta_L = 15^\circ$. As can be seen from the image along with these two samples, five additional samples were measured using our measurement setup, however, it was not possible to have them measured using any of the gonio-spectrophotometers. We therefore use two samples (M and C) in the analysis and comparison. Table 5 gives an overview of the measurement angles and the instruments with which the samples were measured. Figures 6 and 7 show θ_i and θ_r angles at which the samples were measured using both the gonio-spectrophotometers and our measurement setup. Please make a note that GCSM gonio-spectrophotometer measures at 1° near specular angles while at 5° intervals away from the specular direction.

The camera records a 16 bit raw RGB image. To correct for dark current noise we subtract a dark image (captured with camera lens cap on in a dark room) from the captured image. Five vertical pixels from the sample center for the given point (P) are averaged. Camera settings have been similar while measuring the camera spectral sensitivities and while measuring the samples.

In radiometric terms, the 16 bit raw RGB data recorded corresponds to the radiance exited from the curved sample surface (as we work at a constant exposure time, the RGB data recorded

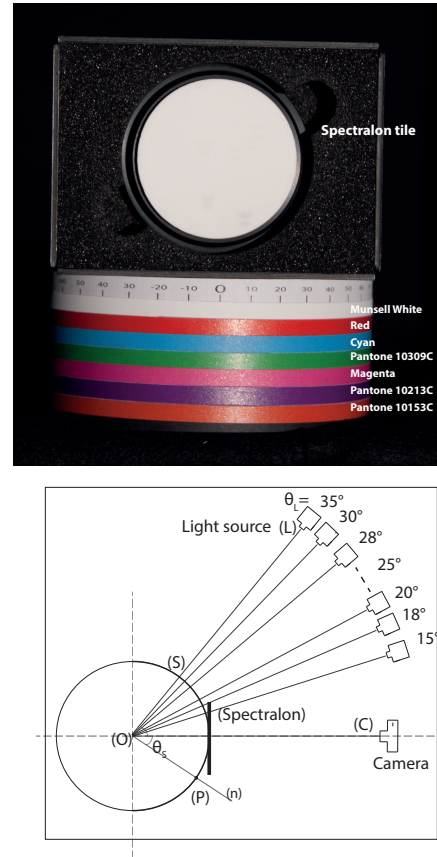


Fig. 4. Sample measurement at 7 different illumination directions (θ_L) and image captured at $\theta_L = 15^\circ$

corresponds to radiance). To compare the measurements made using our measurement setup and gonio-spectrophotometers, we need to either calculate spectral radiance factor from the raw RGB data measurements, or vice versa.

Using the BRDF definition, the radiance exited from the sample surface can be calculated using the sample BRDF measured by the gonio-spectrophotometer. For a small homogeneous area, spectral radiance reflected from the sample surface in a given direction can be defined as given in Equation (4).

$$L_r(\theta_i, \phi_i, \theta_r, \phi_r, \lambda) = f_r(\theta_i, \phi_i, \theta_r, \phi_r, \lambda) \cdot E_i((\theta_i, \phi_i, \lambda)) \quad (4)$$

where, $L_r(\theta_i, \phi_i, \theta_r, \phi_r, \lambda)$ is the spectral radiance exited from the sample, $E_i((\theta_i, \phi_i, \lambda))$ is the spectral irradiance at the sample, and f_r is the sample BRDF (obtained from the gonio-

Measurement device	Data recorded	Samples measured				
		ST	LC	LM	C	M
Measurement setup	Camera RGB	3 + 7 direc (θ_L)	3 direc ($\theta_L = 24.5^\circ, 31.5^\circ, 37^\circ$)		7 direc ($\theta_L = 15^\circ, 18^\circ, 20^\circ, 25^\circ, 28^\circ, 30^\circ, 35^\circ$)	
LAMBDA1050	Spectral BRDF		$\theta_i = 25^\circ, 35^\circ, 45^\circ$		-NM-	
			$\theta_r = [-75^\circ, +75^\circ]$ at 5° interval			
GCSM			-NM-		$\theta_i = \theta_r = [-80^\circ, +80^\circ]$ at 5° interval	
-NM- = Could not be measured						

Fig. 5. Overview of measurement angles and sample measurement

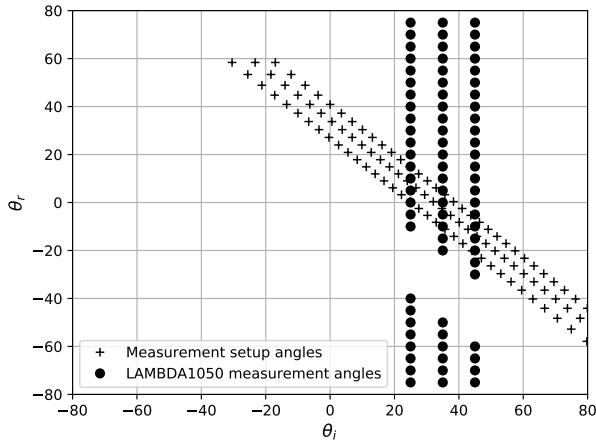


Fig. 6. θ_i and θ_r angles at which LAMBDA1050 and our measurement setup measured

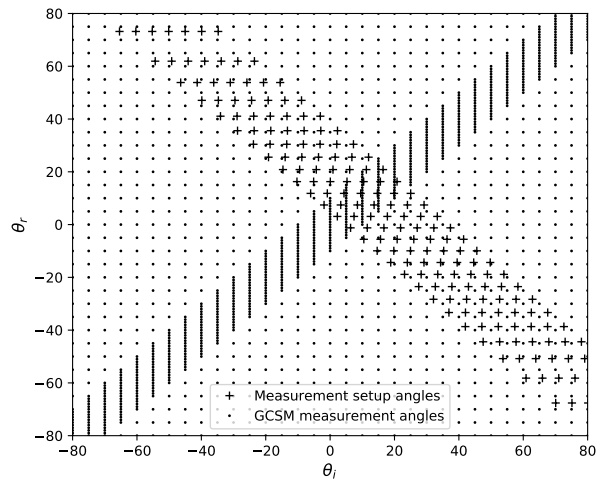


Fig. 7. θ_i and θ_r angles at which GCMS and our measurement setup measured

spectrophotometer measurements). Considering inplane measurements, we re-write Equation (4) using the inverse square law as,

$$L_r(\theta_i, \theta_r, \lambda) = f_r(\theta_i, \theta_r, \lambda) \cdot \frac{I_i(\lambda) \cdot \cos \theta_i}{\omega_s \cdot d^2} \quad (5)$$

where $L_r(\theta_i, \theta_r, \lambda)$ and $f_r(\theta_i, \theta_r, \lambda)$ are as described above in Equation (4) for inplane measurements, $I_i(\lambda)$ is radiant intensity incident normally on the sample, θ_i is anormal incident angle made by the light source relative to the normal at the sample surface, d is distance between sample surface and point light source, and ω_s is the solid angle at the curved sample surface made by the incident light.

In Equation (5), $f_r(\theta_i, \theta_r, \lambda)$ can be measured using a goniospectrophotometer. The incident spectral light intensity, $I_i(\lambda)$ (in our measurement setup), can be calculated using a reference white diffuser such as a Spectralon tile who's BRDF is known for a given θ_i and θ_r and assuming that this reference white diffuser is lambertian. Distance d , will be the distance between point (P) on the curved sample and the point light source in our measurement setup. ω_s will be the solid angle, defined as the ratio of illuminated surface area and square of the distance between the curved surface and light source. We calculate these terms as described below.

Incident spectral light intensity, $I_i(\lambda)$, is estimated using relative normalisation method [25]. The spectralon (ST) BRDF measured with LAMBDA1050 at $\theta_i = 25^\circ$ and $\theta_r = 0^\circ$ is used for the same. Re-writing Equation (5), incident spectral light intensity can be calculated using Equation (6).

$$I_i(\lambda) = \frac{L_{r,spec}(\theta_i=25^\circ, \theta_r=0^\circ, \lambda=380nm-730nm) \cdot d^2}{f_{r,spec}(\theta_i=25^\circ, \theta_r=0^\circ, \lambda=380nm-730nm) \cdot \cos \theta_i} \quad (6)$$

where $L_{r,spec}(\theta_i=25^\circ, \theta_r=0^\circ, \lambda=380nm-730nm)$ is the spectral radiance exited from the spectralon surface and $f_{r,spec}(\theta_i=25^\circ, \theta_r=0^\circ, \lambda=380nm-730nm)$ is the spectral BRDF of the spectralon measured with LAMBDA1050, at the given incident ($\theta_i=25^\circ$) and reflection ($\theta_r=0^\circ$) angle. θ_i and d are the same as defined in Equation (5).

The distance (d), is the distance P_L in our measurement setup vector space (refer Figure 1). d can therefore be calculated using the coordinate values for point P on the curved sample surface and point light source L. We solve for distance P_L (refer Equation (7)) where, d_L is the distance between point light source (L) and origin (O), R is the radius of the cylinder on which the sample is curved, θ_L is the illumination direction angle and θ_S is the angle made by point (P) on the curved sample surface with vector OC.

$$\mathbf{P}_L = [P, D] \quad (7)$$

$$P_L = |P_L| = \sqrt{d_L^2 + R^2 - 2d_LR \cos(\theta_L - \theta_S)}$$

The solid angle, ω_s , can be calculated using the illuminated area and distance between the illuminated sample area and the light source. The distance between the illuminated sample area and the light source is calculated using Equation (7) at each point (P) on the curved sample surface. As we use a film projector to illuminate the curved sample, the area illuminated by the point light source will correspond to the physical area on the curved surface covered by each camera pixel.

To calculate the physical area covered by each pixel on the curved sample surface, we ignore errors due to lens structure in the camera and assume that each pixel of the camera makes same solid angle (ω_r) with respect to the captured image and

the pixel location on the camera sensor. We capture an image of a white patch with the camera that is used in our measurement setup. Assuming the image of the white patch as a single pixel, the solid angle ω_r formed by the camera with respect to the area of the white patch is as given in Equation (8). A_{sq} is the physical area of the white patch (in mm) and d is the distance between the camera and the white surface (in mm).

$$\omega_r = \frac{A_{sq}}{d^2} = \frac{(20 \times 25)}{490^2} = 0.00208 \text{ sr}. \quad (8)$$

Dividing the solid angle with the total number of pixels gives us the solid angle (ω_{r_p}) for each pixel. As distance P_L is known for each point (P) on the curved sample surface, ω_s can be calculated using the surface area covered under each pixel. ω_s remained constant over the pixel position (corresponding to the point P on the sample surface) and therefore was taken into account while calculating $I_i(\lambda)$.

Referring the vector space in Figure 1, distance P_C between the detector and the sample surface is calculated using Equation (9). Note that P_C will change with the location on the sample surface as it is curved due to wrapping around a cylinder of radius R .

$$\mathbf{P}_C = [P, C] \quad (9)$$

$$P_C = |P_C| = \sqrt{d_c^2 + R^2 - 2Rd_c \cos \theta_s}$$

where d_c is the distance between the camera (C) and origin (O), R is the radius of the cylinder on which the sample is curved, and θ_s is the angle made by point (P) on the curved sample surface with vector \mathbf{OC} . As we now know the distance between the camera and the sample surface and the solid angle each camera pixel makes, the physical area covered by each pixel can be calculated using the relation ($Area = \omega \cdot distance^2$).

To compare the measurements, for simplicity of calculations we convert the sample BRDF to camera RGB values. Referring Equation (4), we use the irradiance at the sample surface in our measurement setup to calculate the radiance at the sample surface for the incident (θ_i) and reflection (θ_r) directions at which the sample BRDF is measured using a gonio-spectrophotometer. The light incident on the sample surface, $I_i(\lambda)$, is calculated using Equation (6). The spectral BRDF $f_{r,spec}(\theta_i=25^\circ, \theta_r=0^\circ, \lambda_{400-700})$ is measured using LAMBDA1050 while the spectral surface radiance $L_{r,spec}(\theta_i=25^\circ, \theta_r=0^\circ, \lambda_{400-700})$ is measured using a tele-spectroradiometer (TSR) in our measurement setup. The camera is replaced by the TSR in our measurement setup to measure the radiance. As the remaining parameters of the Equation (5) are known, we can calculate radiance at the sample surface.

As we compare measurements made using two methods, one being radiance L_r , a physical quantity, while other is camera RGB, a relative value, the measured data should be calibrated to the incident light intensity in the setup. We scale the incident light intensity using a camera coefficient g as given in Equation (10). $L_{r,spec}$ is the radiance measured at the spectral surface at $\theta_i=25^\circ, \theta_r=0^\circ, \lambda_{400-700}$ by replacing the camera with a TSR in our measurement setup, while $\bar{g}(\lambda)$ is the spectral sensitivity of the camera green sensor.

$$g = \sum_{\lambda=400}^{700nm} \bar{g}(\lambda) \cdot L_{r,spec}(\lambda) \Delta\lambda_{10nm} \quad (10)$$

Using the BRDF measurements of the sample (measured using a gonio-spectrophotometer), and the scaled incident light intensity ($I_i(\lambda)/g$), the radiance at the sample surface (for the

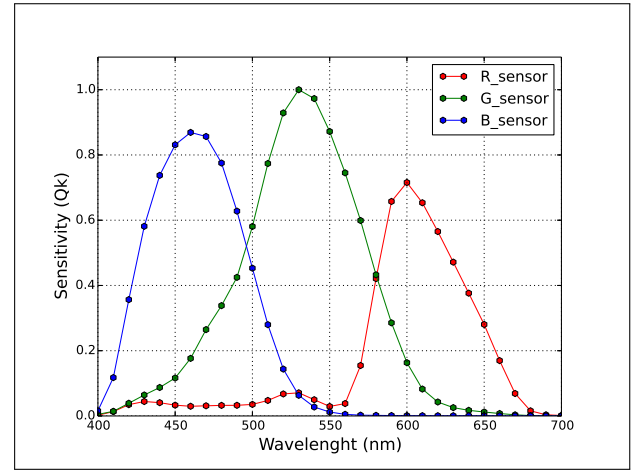


Fig. 8. Camera sensor sensitivity functions [22].

incident (θ_i) and reflection (θ_r) angles at which the BRDF is measured) is calculated using Equation (11).

$$L_r(\theta_i, \theta_r, \lambda) = f_r(\theta_i, \theta_r, \lambda) \cdot \frac{I_i(\lambda)}{g} \cdot \frac{\cos \theta_i}{\omega_s \cdot d^2} \quad (11)$$

The radiance obtained, is then converted to camera RGB values using Equation (12), where $L_r(\theta_i, \theta_r, \lambda)$ is the radiance at the sample surface in our measurement setup calculated using Equation (11) (but for the incident and reflection angles used in gonio-spectrophotometer measurements) and $(\bar{r}, \bar{g}, \bar{b})$ are spectral sensitivities of camera used as a detector in our measurement setup.

$$\begin{pmatrix} Cal_R(\theta_i, \theta_r) \\ Cal_G(\theta_i, \theta_r) \\ Cal_B(\theta_i, \theta_r) \end{pmatrix} = \begin{pmatrix} \sum L_r(\theta_i, \theta_r, \lambda) \cdot \bar{r} \\ \sum L_r(\theta_i, \theta_r, \lambda) \cdot \bar{g} \\ \sum L_r(\theta_i, \theta_r, \lambda) \cdot \bar{b} \end{pmatrix} \quad (12)$$

A point to note here is that when measuring the sample material using a gonio-spectrophotometer, measurements are performed at fixed incidence (θ_i) and reflection (θ_r) angles, while the measurement setup uses a camera, thus capturing the reflected radiance from the sample surface per pixel. In our measurement setup, each pixel corresponds to the point (P) on the curved sample surface that makes an unique incident (θ_i) and reflection (θ_r) angle relative to the surface normal. Using a high resolution camera, the θ_i and θ_r combination is high and different compared to the gonio-spectrophotometer measurements. It records approx. 1000 pixels (horizontally) for each sample.

Another point to note here is that total number of pixels will vary depending upon the radius of the cylinder on which the sample is curved, the distance between the sample and the camera, and the resolution of the camera used in our measurement setup. This data, therefore, being too dense, we use information captured at every 50th pixel for comparison. Depending on the sample material being measured and the interval between the angles required, the pixel interval can be increased or decreased.

We interpolate camera RGB measurements that are calculated using gonio-spectrophotometer measurements using Equation (12) at the incident and reflection angles of our measurement setup. Interpolation is performed using a standard piecewise cubic spline interpolation.

B. Measurement error

Measurement setup has three main components: a camera (as a detector), a point light source (to illuminate the sample), and the sample to be measured (wrapped around a cylinder of known radius). We calculate the incident and reflection angle made by point (P) on the sample with respect to the light direction and the camera position from the curved sample. The incident and reflection angle calculations are therefore dependent on θ_L (light direction with respect to normal to the camera), cylinder radius (R) on which the sample is wrapped, distance (d_L) between curved sample and point light source, distance (d_C) between curved sample and camera, pixel position (d_p) on the camera with respect to point P on the curved sample surface and effective camera focal length (F_p). Also, our measurement setup uses a RGB camera as a detector. The camera used in the setup (Nikon D200) records raw RGB data for the radiance exited from the sample surface. We convert this data to CIE XYZ values using a conversion matrix (\hat{M}). As discussed in [22], \hat{M} is derived using camera sensitivity measured with a monochromator and CIE 2° colour matching functions. Figure 8 shows the sensitivities (measured using the monochromator) of the camera used in our measurement setup. Calculating CIE XYZ values with \hat{M} introduces error in the colorimetric values. It is therefore important to take into account the uncertainty (in terms of measurement error) in these calculations when comparing with the gonio-spectrophotometer measurements.

We derive error uncertainty in calculating incident (θ_i) and reflection (θ_r) angles using the procedure given by the Joint Committee for Guides in Metrology (JCGM) [26].

$$\Delta\theta_{S_{edge}} = \sqrt{\left(\frac{\partial\theta_{S_{edge}}}{\partial d_C} \cdot \Delta d_C\right)^2 + \left(\frac{\partial\theta_{S_{edge}}}{\partial R} \cdot \Delta R\right)^2}$$

$$\frac{\partial\theta_{S_{edge}}}{\partial d_C} = \frac{-1}{\sqrt{\left(1 - \left(\frac{d_C}{R}\right)^2\right)}} \cdot \frac{1}{R} \quad (13)$$

$$\frac{\partial\theta_{S_{edge}}}{\partial R} = \sqrt{\left[\frac{-\Delta d_C}{R \cdot \sqrt{1 - \left(\frac{d_C}{R}\right)^2}}\right]^2 + \left[\frac{d_C \cdot \Delta R}{R^2 \cdot \sqrt{1 - \left(\frac{d_C}{R}\right)^2}}\right]^2}$$

Equation (13) shows the uncertainty in calculating $\theta_{S_{edge}}$. Calculations of $\theta_{S_{edge}}$ can be referred in [19]. $\theta_{S_{edge}}$ is the θ_S angle at the edge of the curved sample when viewed from the camera field of view. In the same way, uncertainty in θ_i , θ_r , θ_S and F_p is derived and is approximated for the physical measurements Δd_L , Δd_C , $\Delta\theta_S$, ΔR and $\Delta\theta_L$. Equation (14) calculates the error in CIE Y calculation using values that are calculated using

- \hat{M} and RGB values calculated using Equation (12) and,
- L_r calculated using Equation (11) and CIE 2° colour matching functions.

$$\Delta Y = \frac{\sqrt{(Y_{(\hat{M}-RGB)} - Y_{(L_r-CIE2^\circ)})^2}}{Y_{(L_r-CIE2^\circ)}} \quad (14)$$

The two samples LightCyan (LC) and LightMagenta (LM), and the spectralon tile (ST) were measured using LAMBDA1050 at three anormal incident ($\theta_i = 25^\circ, 35^\circ, 45^\circ$) and 26 anormal reflection angles (ranging between $\theta_r = [+75^\circ, -75^\circ]$ at 5° intervals) while two samples Cyan (C) and Magenta (M) using GCMS

in the range of $\theta_i = \theta_r = [+80^\circ, -80^\circ]$ at 5° intervals. All the samples were measured using our measurement setup at different incident light directions (θ_L).

We interpolate measurements conducted with gonio-spectrophotometer at angles (θ_i and θ_r) measured at by our measurement setup. Point to note here is that the measurements we interpolate here are camera RGB values converted (using Equation (12)) from the BRDF measurements performed by the gonio-spectrophotometers. CIE XYZ values were further calculated from the interpolated RGB measurements using the conversion matrix (\hat{M}). The spectralon tile measurements at $\theta_L = 25^\circ$ was used as reference white measurement with CIE Y value as 1.0.

To evaluate the setup we analyse the calculated CIE Y value (hereby referred as luminance value). Relative ΔY error is calculated for each sample between the gonio-spectrophotometer and measurement setup measurements using Equation (15).

$$Error_{\Delta Y} = \frac{\sqrt{(Y_{Gonio} - Y_{Setup})^2}}{Y_{Gonio}} \quad (15)$$

where, Y_{Gonio} is the luminance value calculated using measurements performed by the gonio-spectrophotometer and Y_{Setup} is the luminance value calculated using the measurements from our measurement setup of the respective sample material.

3. RESULTS

Table 1 shows the uncertainty derived and approximated for our measurement setup parameters. Table 2 shows the uncertainty in CIE Y calculations.

Table 1. Measurement uncertainty in our measurement setup parameters

	Setup parameters	Uncertainty
Calculated	θ_i	$\pm 7.6^\circ$
	θ_r	$\pm 7.4^\circ$
	θ_S	$\pm 6.7^\circ$
	F_p	± 1973 pixels
Approximated	R	± 5 mm
	d_C	± 10 mm
	d_p	± 5 pixels
	d_L	± 20 mm
	θ_L	$\pm 4^\circ$

Table 2. Error (ΔY) in CIE Y calculation

Sample	LC	LM	C	M
ΔY	0.11	0.12	0.18	0.13

The average $Error_{\Delta Y}$ for each sample material is calculated (refer Table 3). Figure 9 - 12 shows the calculated luminance for the samples against the reflection angles at respective incident

Table 3. $Error_{\Delta Y}$ between luminance calculated using measurements from our measurement setup and gonio-spectrophotometer

Instrument	θ_L	LC sample	LM sample
LAMBDA1050	24°	0.12	0.01
	34°	0.14	0.01
	44°	0.18	0.15
	Average	0.14	0.05
Instrument	θ_L	C sample	M sample
GCSM	15°	0.21	0.19
	18°	0.21	0.19
	20°	0.21	0.20
	25°	0.22	0.21
	28°	0.24	0.22
	30°	0.27	0.22
	35°	0.32	0.29
	Average	0.24	0.21

light direction along with the measurement uncertainty in calculating the angles and CIE Y values. Note that as the number of incident light directions (θ_L) used and samples measured being many when comparing against GCSM measurements, we show results for the measured samples at one incident directions ($\theta_L = 35^\circ$). For comparison with LAMBDA1050 measurements we show results for both the samples (LC, LM) for one incident light direction ($\theta_L = 44^\circ$).

Looking at the plots we can observe that the measurements performed using the gonio-spectrophotometers lie within a known uncertainty of our measurement setup for the samples used in this study.

4. DISCUSSION

Samples LM and LC were measured at three incident angles (θ_i) using LAMBDA1050 and three light direction (θ_L) in our measurement setup. Due to measurement setup limitations and the limited measurements from LAMBDA1050, the measurement region of overlap in terms of θ_i and θ_r were limited (refer Figure 6). It was therefore possible to compare only a limited number of measurements for the LC and LM samples. Point to note here is that we perform a relative comparison using BRDF measurement of the spectralon tile (at $\theta_i=25^\circ$, $\theta_r=0^\circ$) to normalise both the measurements. Similar comparison is done for the C and M samples measured with GCSM. With GCSM, it was possible to measure the entire plane for incident and reflection angles at 5° interval (refer Figure 7). Same samples were measured at seven different incident light directions (θ_L) using our measurement setup in order to have a bigger overlap in the measurement region (with respect to θ_i and θ_r directions) compared to the measurements performed using LAMBDA1050 for LC and LM samples. The average ΔY between the measurements was highest for the C sample compared to other samples. The measurement setup we evaluate in this article has different components. We calculated the error in incident and reflection

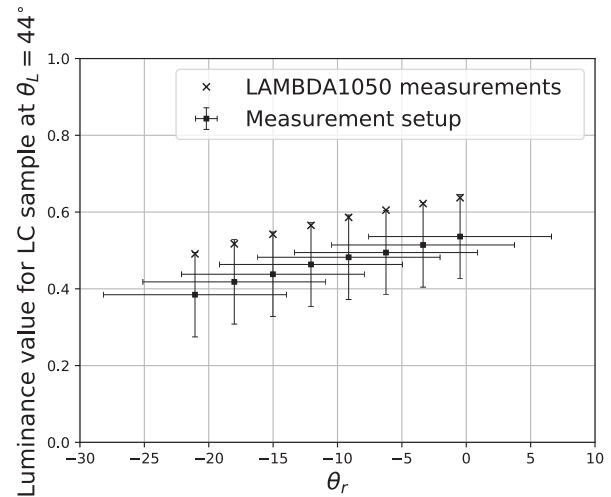


Fig. 9. Calculated luminance (Y) values for LC sample for measurements at $\theta_L = 44^\circ$, using our measurement setup and LAMBDA1050 against θ_r

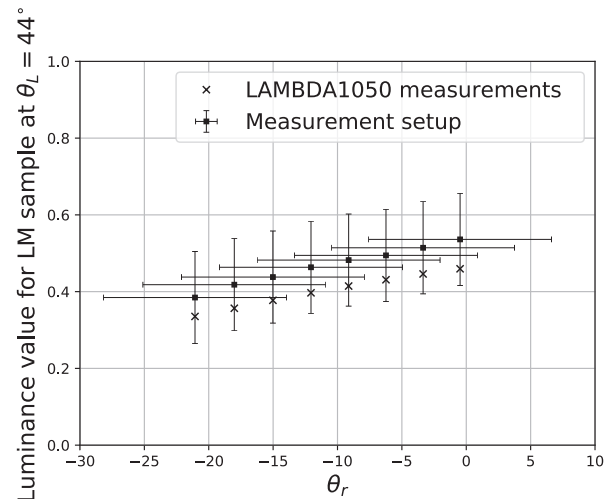


Fig. 10. Calculated luminance (Y) values for LM sample for measurements at $\theta_L = 44^\circ$, using our measurement setup and LAMBDA1050 against θ_r

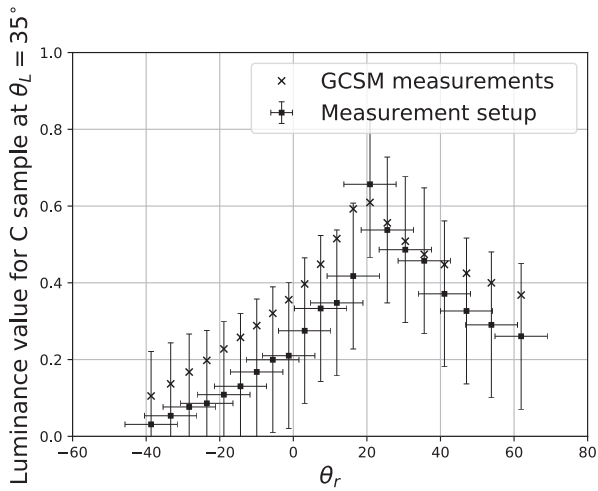


Fig. 11. Calculated luminance (Y) values for C sample for measurements at $\theta_L = 35^\circ$, using our measurement setup and GSCM against θ_r

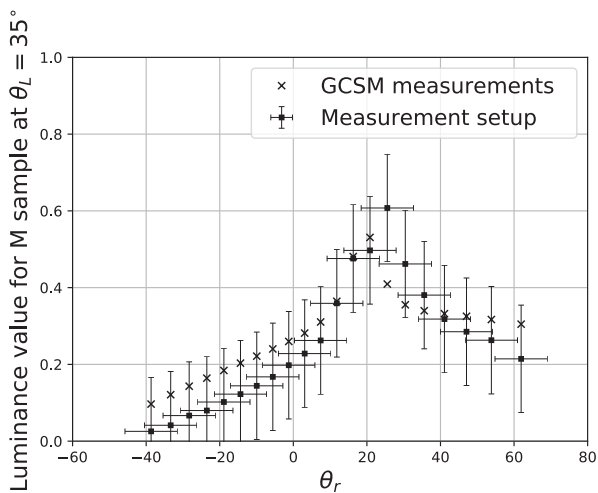


Fig. 12. Calculated luminance (Y) values for M sample for measurements at $\theta_L = 35^\circ$, using our measurement setup and GSCM against θ_r

angle calculations and, CIEXYZ calculations from the camera RGB.

Error in physical measurements (cylinder radius (R), distance between the curved sample and the detector (d_C), distance between the curved sample and the light source (d_L), and angles between d_C and d_L (θ_L)) contribute to the error in estimating the incident and reflection angles at point (P) on the curved sample surface. The uncertainty in estimating θ_i and θ_r is large. We observed that the uncertainty in calculating θ_i and θ_r angles is more sensitive to physical measurements d_C , d_L and θ_L compared to the radius (R) of the cylinder.

To calculate colorimetric values we use the conversion matrix (\hat{M}) along with camera measurements. \hat{M} is calculated using least square error between the camera sensitivity functions and the CIE 2° colour matching functions. Depending on the colour of the sample being measured, conversion from camera RGB to CIEXYZ will introduce an error in the colorimetric values due to matrix (\hat{M}). We calculated this error by comparing the luminance (CIE Y) values calculated using a) the camera measurements and matrix (\hat{M}) and, b) radiance values and the colour matching functions.

Figures 9 – 12 show the comparison of measurements using the measurement uncertainty (in the form of error bars) of our measurement setup. An important point to understand from these plots is that as long as the measurements obtained from the gonio-spectrophotometer are within the uncertainty of our measurement setup, it should be possible to use our measurement setup to perform multi-angle BRDF measurements with a known uncertainty to measure materials similar to the sample material used in this study. Another point to consider is that we have not taken into account the measurement uncertainty of the gonio-spectrophotometers used in this study. Measurement uncertainty provided by the manufacturer of these instruments is usually for one incident and reflection angle and for one wavelength interval (for example $\theta_i = 45^\circ$, $\theta_r = 0^\circ$, $\lambda = 560$ nm). To calculate the instrument uncertainty with the aim to compare with the camera setup, it would require a number of approximations to be made which would then add to the comparison error that would be difficult to eliminate. Also, it is expected that the gonio-spectrophotometers are much more accurate compared to our setup and therefore the uncertainty of our setup is calculated and analysed.

Looking at the results obtained for the samples used, luminance (CIE Y) measured using the gonio-spectrophotometer lies within the measurement uncertainty of our measurement setup. For the LC sample measured at $\theta_L = 44^\circ$, the error is maximum. Although similar observation can be made for C sample, the measurements are well within our measurement setup uncertainty. The possible reason for having a large error in the cyan samples is the camera sensor limitations in the blue spectrum. It is also observed that, as the incident light direction (θ_L) increases, we observe an increase in the error value between the measurements especially for LC and C samples but also for LM and M samples. Increasing θ_L contributes to the error due to geometrical calibration and uncertainty in physical measurements of the setup. Also, the sample being curved, bigger the θ_L , more are the incident and reflection directions for given point P on the sample surface.

From the plots (Figures 9 – 12) we can observe that the measurements performed using our measurement setup show lower CIE Y values compared to gonio-spectrophotometer measurements for LC and C samples. However, for LM sample our measurement setup measures a higher CIE Y compared

to the gonio-spectrophotometer measurements. For sample M, the measurements from our measurement setup and gonio-spectrophotometer do not follow a systematic curvature as seen for the other samples (LC, C and LM). The measurement setup measurements show a lower CIE Y value for reflection angles in an approximate range of -40° to 10° and a higher CIE Y value from approximately $\theta_r = 25^\circ$ to 40° .

The possible reason for such a systematic behaviour can be the error in calculating CIE Y value from camera RGB values using the conversion matrix \hat{M} . \hat{M} is calculated using the camera spectral sensitivities and the CIE 2° colour matching functions. In the CIExyY colorimetric space, the camera sensitivity values will correspond to the points on the locus of the chromaticity diagram. The error in calculating CIE Y value from camera RGB will therefore depend on the colour sample being converted. These points need a thorough investigation and will be future work for the authors.

From the achieved results can we question if this uncertainty is sufficiently low for a practical use of our measurement setup? The practical use will depend on a) the type of material being measured, b) the measurement accuracy required, and c) implications of the performed measurements. Given the measurement uncertainty, our measurement setup can be used by customers for fast measurements to understand bidirectional material properties and material visualisation. With the obtained uncertainty our measurement setup will not be suitable for precise measurements for applications like security, medical or measurement traceability.

5. CONCLUSIONS

In this article, we evaluate an image based multi-angle measurement setup against commercially available table-top gonio-spectrophotometers for bidirectional measurements of flexible and homogeneous materials. We measure four samples using our measurement setup and two gonio-spectrophotometers at different incident and reflection directions.

Measurement setup can perform multi-angle BRDF measurements but with a large uncertainty. Gonio-spectrophotometer measurements lie within the measurement uncertainty of our measurement setup. The uncertainty in calculating θ_i and θ_r is large and more precise measurements of the physical parameters are required. Measurement setup can be used to measure (with known uncertainty) materials similar to the sample material used in this article. The setup can be used for fast multi-angle measurements however with a known uncertainty. Due to fast measurements using the setup, it can also help automate in-line multi-directional measurements during reproduction of packaging materials like the ones used in this study.

APPENDIX

PerkinElmer's LAMBDA1050 gonio-spectrophotometer

PerkinElmer's LAMBDA1050 gonio-spectrophotometer contains ARTA accessory from OMT Solutions BV. The sample to be measured is illuminated with a monochromatic light. Light source used is a tungsten halogen light bulb. It is a double beam instrument, with the reference beam leading directly to the detector, thus measuring the incident radiant flux (Φ_i) in watts. It uses a double holographic grating monochromator to have a monochromatic light from the light beam incident on the sample. The sample is positioned on a rotating stage, and the angle of incidence (measured from the normal to the sample

surface) is varied by rotating the sample using a motor. The light reflected from the sample is detected with an integrating sphere detector of diameter 60 mm and consists of a photomultiplier tube as a detector. The detector revolves around the sample and can be positioned at angles relative to normal of sample surface, except for $\pm 10^\circ$ near the light source. The measurement output of this instrument is the ratio of reflected radiant flux to incident radiant flux. This instrument has been used previously [23] to study the angular variations in reflectance and fluorescence from paper that contain fluorescent whitening agents and fillers. Please refer PerkinElmer's LAMBDA1050 manual¹ for details and specifications of LAMBDA1050.

Murakami's GCMS-3B Gonio-spectrophotometric Color Measurement System

Murakami's GCMS-3B Gonio-spectrophotometric Color Measurement System also has a double beam design wherein the radiant flux reflected from the sample material is continuously compared with against measurements made on a reference white diffuser plate. The light source is a tungsten halogen light bulb at a fixed position, while the detector (Silicon Photo-diode array) revolves around the sample within the range of anormal angles $\pm 80^\circ$ to the sample plane (when normal to the incident light). The sample to be measured is mounted on a flat plate which again rotates between anormal angles $\pm 80^\circ$ with respect to the incident light source normal to the sample plane. The light beam is divided into 2 identical beams using mirrors, lenses and heat filters to simultaneously illuminate the sample and the white reference plate. The instrument automatically corrects for the variation in intensity, and the area of illumination/viewing, due to the rotation of the plate and the detector. The measurement output of this device is radiance factor (β) measurement. As the reference white plate used in the measurement is assumed as a perfect reflecting diffuser, we can calculate the BRDF of the sample using $\beta = \pi \cdot f_r$ relation. Please refer to Murakami's GCMS-3B Gonio-spectrophotometric Color Measurement System manual² for details and specifications of this instrument.

ACKNOWLEDGMENT

We would like to thank and acknowledge support of Dr. Reiner Eschbach, Dr. Jean-Baptiste Thomas and Dr. Giuseppe Claudio Guarnera, at the Norwegian Colour and Visual Computing Laboratory in discussions and suggestions regarding the structure of this paper.

This work was supported by the MUVApp project N-250293, funded by the Research Council of Norway.

REFERENCES

1. C. Eugène, "Measurement of "total visual appearance": a cie challenge of soft metrology," in "12th IMEKO TC1 and TC7 Joint Symposium on Man, Science and Measurement," (Annecy, France, 2008), pp. 61 – 65.
2. G. Pfaff, *Special effect pigments: technical basics and applications* (Vincentz Network GmbH & Co KG, 2008).
3. P. Pjanic and R. D. Hersch, "Specular color imaging on a metallic substrate," in "Color and Imaging Conference," (Society for Imaging Science and Technology, 2013), pp. 61–68.

¹Lambda 1050 uv/vis/nir spectrophotometer, <http://www.perkinelmer.com/product/lambda-1050-uv-vis-nir-spectrophotometer-l1050?searchTerm=L1050&pushBackUrl=?searchName=L1050>. Accessed:2017-03-09.

²Gcms-3 goniospectrophotometer system, http://www.aviangroupusa.com/pdf/GCMS3_Des.pdf. Accessed: 2017-03-09.

4. C. McCamy, "Observation and measurement of the appearance of metallic materials. part i. macro appearance," *Color Research & Application* **21**, 292–304 (1996).
5. A. Takagi, S. Sato, and G. Baba, "Prediction of spectral reflectance factor distribution of color-shift paint finishes," *Color Research & Application* **32**, 378–387 (2007).
6. E. Kirchner and W. Cramer, "Making sense of measurement geometries for multi-angle spectrophotometers," *Color Research & Application* **37**, 186–198 (2012).
7. A. Ferrero, A. Rabal, J. Campos, F. Martínez-Verdú, E. Chorro, E. Perales, A. Pons, and M. L. Hernanz, "Spectral brdf-based determination of proper measurement geometries to characterize color shift of special effect coatings," *J. Opt. Soc. Am. A* **30**, 206–214 (2013).
8. CIE15.2, "Colorimetry," CIE standard (2004).
9. ASTM-E2194, "Standard practise for multiangle color measurement of metal flake pigmented materials," ASTM Standard (2012).
10. ASTM-E2539, "Standard practise for multiangle color measurement of interference pigments," ASTM Standard (2012).
11. C. McCamy, "Observation and measurement of the appearance of metallic materials. part ii. micro appearance," *Color Research & Application* **23**, 362–373 (1998).
12. ASTM-E2175, "Standard practice for specifying the geometry of multi-angle spectrophotometers," ASTM Standard (2013).
13. K. Kehren, "Optical properties and visual appearance of printed special effect colors," Ph.D. thesis, Technischen Universität Darmstadt, Darmstadt, Germany (2013).
14. J. Palmer and B. G. Grant, *The Art of Radiometry*, ISBN 978-0-8194-7245-8 (SPIE Press Bellingham, Washington USA, 2010).
15. F. E. Nicodemus, J. Richmond, J. J. Hsia, I. W. Ginsberg, and T. Limperis, "Geometrical considerations and nomenclature for reflectance," National Bureau of Standards (1977).
16. CIE175, "A framework for the measurement of visual appearance," Tech. rep., International Commission on illumination (2006).
17. S. Tominaga and N. Tanaka, "Estimating reflection parameters from a single color image," *IEEE Computer Graphics and Applications* **20**, 58–66 (2000).
18. D. Guarnera, G. Guarnera, A. Ghosh, C. Denk, and M. Glencross, "Brdf representation and acquisition," *Computer Graphics Forum* **35**, 625–650 (2016).
19. A. Sole, I. Farup, and S. Tominaga, "An image based multi-angle method for estimating reflection geometries of flexible objects," *Color and Imaging Conference* **2014**, 91–96 (2014-11-03T00:00:00).
20. A. S. Sole, I. Farup, and S. Tominaga, "An image-based multi-directional reflectance measurement setup for flexible objects," in "Measuring, Modeling and Reproducing Material Appearance 2015," , vol. SPIE 9398 M. V. O. Segovia, P. Urban, and F. H. Imai, eds. (Proceedings of SPIE-IS& T Electronic Imaging, 2015), vol. SPIE 9398, pp. 93980J – 93980J–11.
21. A. Sole, I. Farup, and P. Nussbaum, "Evaluating an image based multi-angle measurement setup using different reflection models," *Electronic Imaging* **2017**, 101–107 (2017).
22. A. Sole, I. Farup, and S. Tominaga, "Image based reflectance measurement based on camera spectral sensitivities," *Electronic Imaging* **2016**, 1–8 (2016).
23. N. Johansson and M. Andersson, "Angular variations of reflectance and fluorescence from paper—the influence of fluorescent whitening agents and fillers," in "Color and Imaging Conference," , vol. 2012 (Society for Imaging Science and Technology, 2012), vol. 2012, pp. 236–241.
24. N. Johansson, M. Neuman, M. Andersson, and P. Edström, "Influence of finite-sized detection solid angle on bidirectional reflectance distribution function measurements," *Appl. Opt.* **53**, 1212–1220 (2014).
25. H. Li, S.-C. Foo, K. E. Torrance, and S. H. Westin, "Automated three-axis gonioreflectometer for computer graphics applications," *Optical Engineering* **45**, 043605–043605 (2006).
26. J. C. for Guides in Metrology, "Evaluation of measurement data - guide to the expression of uncertainty in measurement," First edition 100, JCGM (2008).